Electronic Supplementary Material (ESI) for ChemComm.

Hysteretic spin crossover driven by anion conformational change

Natnaree Phukkaphan,[a] Dyanne Cruickshank,[b] Keith S. Murray,[c]

Wasinee Phonsri,[c] Phimphaka Harding[a] and David J. Harding*[a]

E-mail: hdavid@g-mail.wu.ac.th

[a] *Functional Materials and Nanotechnology Centre of Excellence (FuNTech), Walailak University, Thasala, Nakhon Si Thammarat, 80160, Thailand.*

[b] *Rigaku Oxford Diffraction, Kemsing, Sevenoaks, TN15 6QY, United Kingdom.*

[c] *School of Chemistry, Monash University, Clayton, Melbourne, Victoria, 3800, Australia.*

Contents

Experimental Procedures

General Remarks Hqsal-I was prepared as previously reported.[1] All other chemicals were purchased from Sigma-Aldrich Chemical Company or TCI Chemicals and used as received. All compounds were prepared in air using reagent grade solvents. Elemental analyses were carried out on a Eurovector EA3000 analyser by staff of the School of Chemistry, University of Bristol, UK. ESI-MS were carried out on a Bruker Daltonics 7.0T Apex 4 FTICR Mass Spectrometer by staff at the National University of Singapore.

[Fe(qsal-I)$_2$]NTf$_2$ [Fe(qsal-I)$_2$]NO_3 was prepared by mixing a CH_2Cl_2 solution of Hqsal-I (374 mg, 1.0 mmol) with a MeOH solution of $Fe(NO_3)_3{\cdot}9H_2O$ (202 mg, 0.5 mmol) and then adding NEt_3 (139 μl, 1.0 mmol). This lead to formation of microcrystals of [Fe(qsal-I)$_2$]NO_3 (410 mg, 0.47 mmol) which were isolated by filtration. [Fe(qsal-I)$_2$]NO_3 was dissolved in heated MeOH (8 ml) to give a black solution. $LiNTf_2$ (136 mg, 0.47 mmol) was dissolved in MeOH (2 ml) and added dropwise to the [Fe(qsal-I)$_2$]NO_3 solution resulting in almost immediate precipitation of a dark brown solid which was collected by filtration and washed with cold MeOH (3 x 3 ml). The solid was redissolved in a 1:1 MeCN:CH_2Cl_2 solution (20 ml in total) filtered through celite and then left to evaporate slowly giving thin black needles (304 mg, 60% yield based on [Fe(qsal-I)$_2$]NO_3). MS (ESI) m/z = 802.0 $[Fe(qsal\text{-}I)_2]^+$, $[NTf_2]^-$ = 279.9. Elemental analysis: calculated for $C_{34}H_{20}F_6FeI_2N_5O_6S_2$: C 37.72 H 1.86, N 6.47%; found C 38.14 H 1.79, N 6.93%.

SQUID magnetometry and DSC measurements

Data were collected using a Quantum Design MPMS 5 SQUID magnetometer under an applied field of 0.5 T over the temperature range 170-350 K. The crystalline samples were placed in gel capsules and care was taken to allow long thermal equilibration times at each temperature point. Data was recorded at 5 and 10 K min^{-1}.

Table S1 Selected examples of Fe(III) and Fe(II) SCO compounds with broad hysteresis.

Compound	Type of SCO	T_{ave} (K)[a]	ΔT	Notes
$[Fe(qsal\text{-}I)_2]NTf_2$	Abrupt	261	34	This work
$[Fe(qsal)_2]NCSe$[2]	Abrupt, 2 step in heating mode	247	3, 70	Stepped SCO shrinks the useable range
$[Fe(qsal)_2]NCS$[3]	Moderately abrupt 2 step in cooling and heating modes	246	87[b]	Stepped SCO shrinks the useable range
β-$[Fe(qsal)_2]I_3$[4]	Abrupt	105	25	Polymorphism makes synthesis problematic
$[Fe(qsal\text{-}I)_2]OTf{\cdot}EtOH$[5]	Abrupt	179	80	Ageing, phase changes and ultimate solvent loss results in variable hysteresis
$[Fe(qnal\text{-}7\text{-}OMe)_2]BPh_4{\cdot}2MeOH$[6]	Abrupt in cooling mode, more gradual in heating mode	249	110[b]	Solvent loss effects unknown
$Li[Fe(5\text{-}Brthsa)_2]{\cdot}H_2O$[7]	Abrupt (heating), gradual (cooling)	~313	39[b]	Impact of solvent loss unknown
$K[Fe(5\text{-}Brthsa)_2]$[8]	Abrupt 2 step	315	52	Stepped SCO slightly limits the useable range
$[Fe(Hthsa)(thsa)]{\cdot}H_2O$[9,10]	Abrupt, 2 steps in cooling mode	253	42	Other reports show abrupt SCO with ΔT = 12 K, suggesting strong sample dependence
$[Fe(L1)(Him)_2]$[11]	Abrupt	279	70	Sample very sensitive to the amount of imidazole present.
$[Fe(L2)(pina)]_n{\cdot}xH_2O{\cdot}MeOH$[12]	Abrupt	288	88	Impact of solvent loss unknown.
$[Fe(NCSe)_2(PM\text{-}PEA)_2]$[13]	Abrupt	286	41	-

[a]An average of the $T_{1/2}$ (↓) and $T_{1/2}$ (↑). [b]At its widest point. [c]L1 = R = OEt; L2 = R = Me;

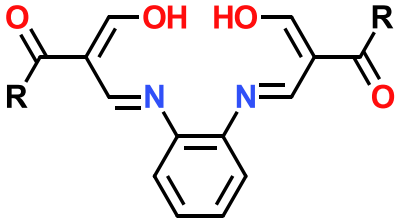

pina = *N*-(pyrid-4-yl)isonicotinamide.

[d] PM-PEA = *N*-(2′-pyridylmethylene)-4-(phenylethynyl)aniline.

DSC measurements were performed using a DSC Q100 V9.9 Build 303 Version 1.0 at a heating or cooling rate of 10 °C min^{-1} over the temperature range 233-353 K. A typical DSC plot is shown in Figure S1.

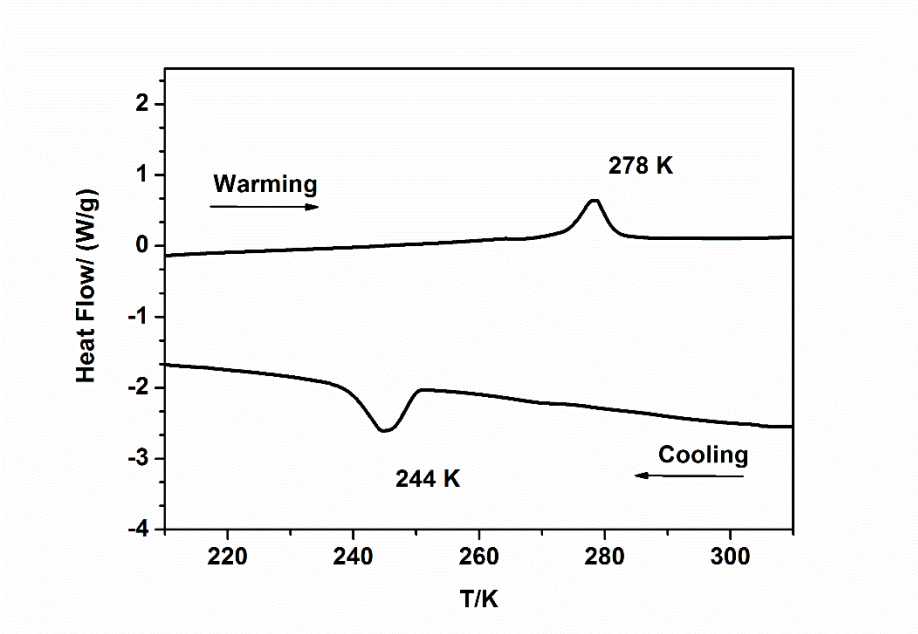

Figure S1 DSC plot of $[Fe(qsal\text{-}I)_2]NTf_2$.

Table S2 Enthalpy and entropy averaged over four cycles in the cooling and warming mode for **1**.

	ΔH (kJ/mol)	ΔS (J/mol·K)
Warming mode	3.946	14.18
Cooling mode	6.038	24.78

Crystal Data and Structures

Single crystal X-ray diffraction data was collected using a Rigaku Oxford Diffraction XtaLAB Synergy-S diffractometer equipped with a HyPix-6000HE photon counting detector. The data were collected upon cooling at 275, 255 and 245 K. Cu radiation (λ = 1.54184 Å) was used for all experiments and the data collection strategy involved several ω scans to achieve a completeness of over 99 % to a resolution of 0.837 Å for all datasets. The software program CrysAlis^{Pro} (Version 1.171.39)[14] was used for data collection and processing. After integration and scaling absorption correction methods were applied which included applying a numerical absorption correction based on gaussian integration over a multifaceted crystal model as well as empirical absorption correction using spherical harmonics as implemented in SCALE3

ABSPACK scaling algorithm. The structures were solved using ShelXT[15] and refined using ShelXL.[16] All pictures were drawn using OLEX2.[17]

Table S3 Crystallographic data and refinement parameters for **1** at 245, 255 (upon cooling from 275 K) and 275 K.

Empirical Formula	$C_{34}H_{20}F_6FeI_2N_5O_6S_2$	$C_{34}H_{20}F_6FeI_2N_5O_6S_2$	$C_{34}H_{20}F_6FeI_2N_5O_6S_2$
Formula Weight	1082.32	1082.32	1082.32
Temperature /K	**245**	**255**	**275**
Crystal System	Triclinic	Triclinic	Triclinic
Space Group	$P\bar{1}$	$P\bar{1}$	$P\bar{1}$
a, b, c /Å	12.4339(13), 12.7007(13), 12.9423(13)	12.3138(3), 12.7727(4), 13.6913(4)	12.3597(3), 12.7897(3), 13.7188(3)
α, β, γ /°	78.012(9), 68.748(10), 68.609(10)	68.975(3), 79.325(2), 66.548(3)	68.956(2), 79.436(2), 66.531(3)
Volume /Å^3	1766.9(4)	1841.71(11)	1854.50(9)
Z	2	2	2
ρ_{calc} /gcm^{-3}	2.034	1.952	1.938
μ /mm^{-1}	19.026	18.253	18.127
F(000)	1050	1050	1050
Crystal Dimensions (mm)	0.033 x 0.047 x 0.215	0.028 x 0.042 x 0.227	0.057 x 0.067 x 0.247
2θ range for data collection /°	7 - 134	7 - 140	7 - 140
Index ranges	-14 ≤ h ≤ 14, -15 ≤ k ≤ 15, -15 ≤ l ≤ 15	-15 ≤ h ≤ 14, -15 ≤ k ≤ 15, -16 ≤ l ≤ 14	-14 ≤ h ≤ 15, -15 ≤ k ≤ 15, -16 ≤ l ≤ 9
Reflections Collected	15216	18864	19970
Unique Data	6074 [R_{int} = 0.0545]	6937 [R_{int} = 0.0398]	6966 [R_{int} = 0.0356]
Data/Restraints/Parameters	6074/0/505	6937/0/505	6966/0/506
Goodness of fit on F^2	1.057	1.056	1.05
Final R factors [I>2σ (I)]	R_1 = 0.0592, wR_2 = 0.1568	R_1 = 0.0441, wR_2 = 0.1197	R_1 = 0.0493, wR_2 = 0.1377
Largest residual peak/hole /eÅ^{-3}	1.181 / -1.361	1.26 / -1.092	1.151 / -1.158
CCDC no.	1552831	1552832	1552833

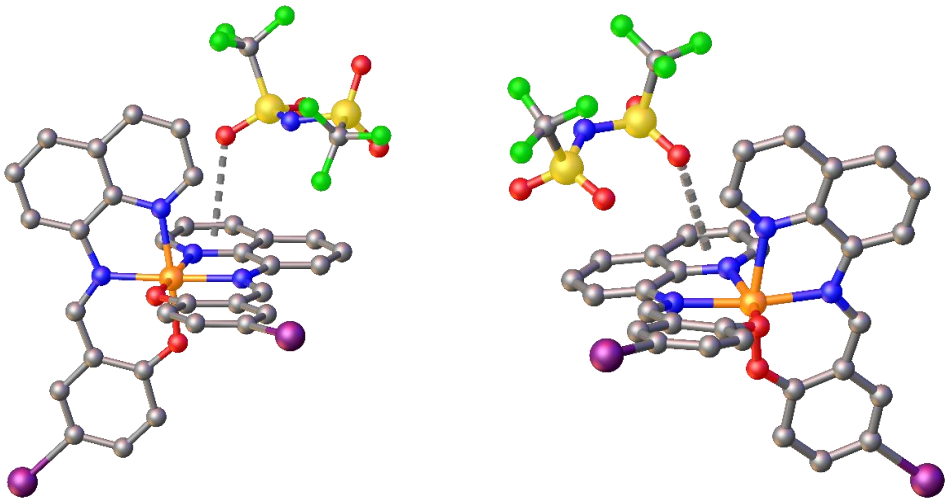

Figure S2 View of the O···π interaction in $[Fe(qsal\text{-}I)_2]NTf_2$ at 245 K (right) and 255 K (left).

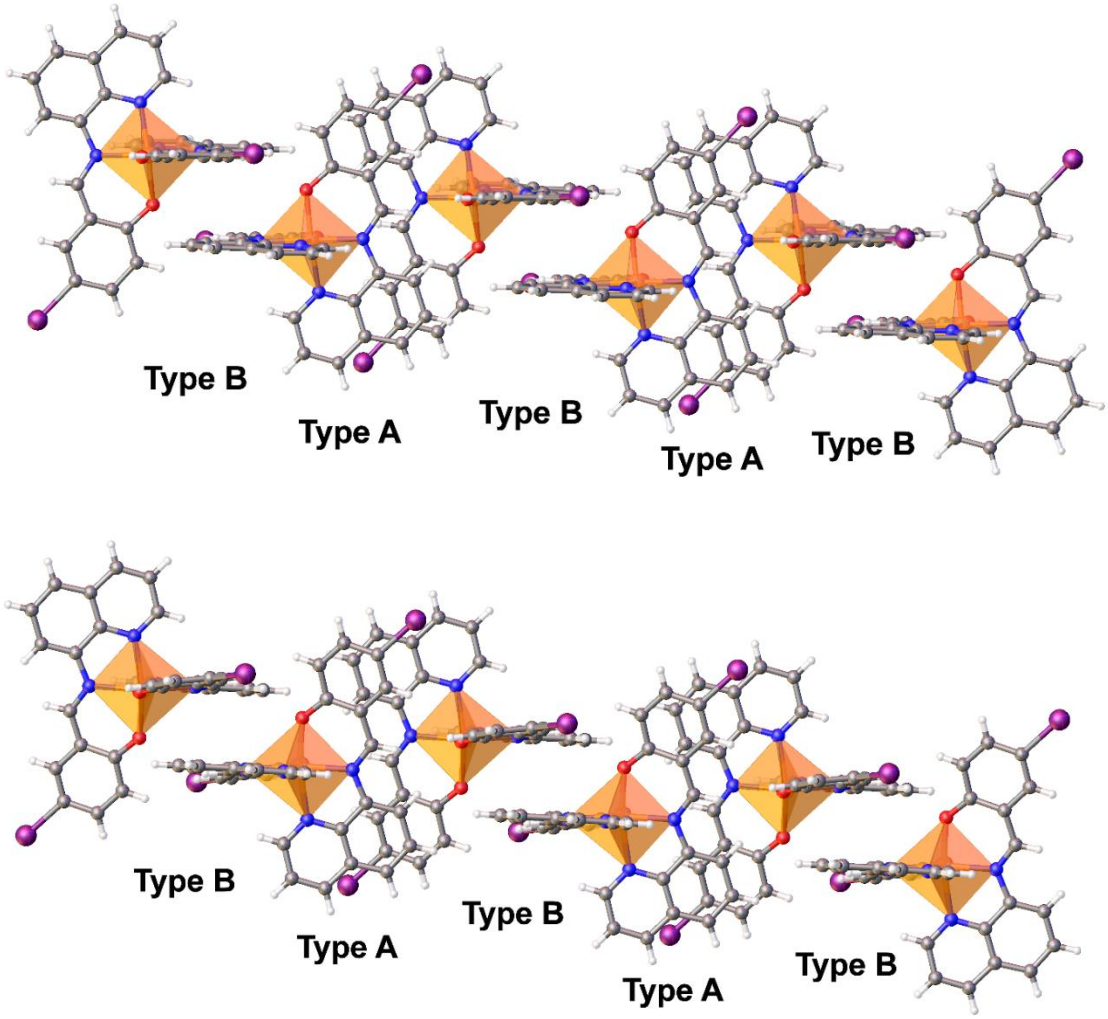

Figure S3 View of the type A and type B π-π interactions in $[Fe(qsal\text{-}I)_2]NTf_2$ in the LS (top) and HS (bottom) state.

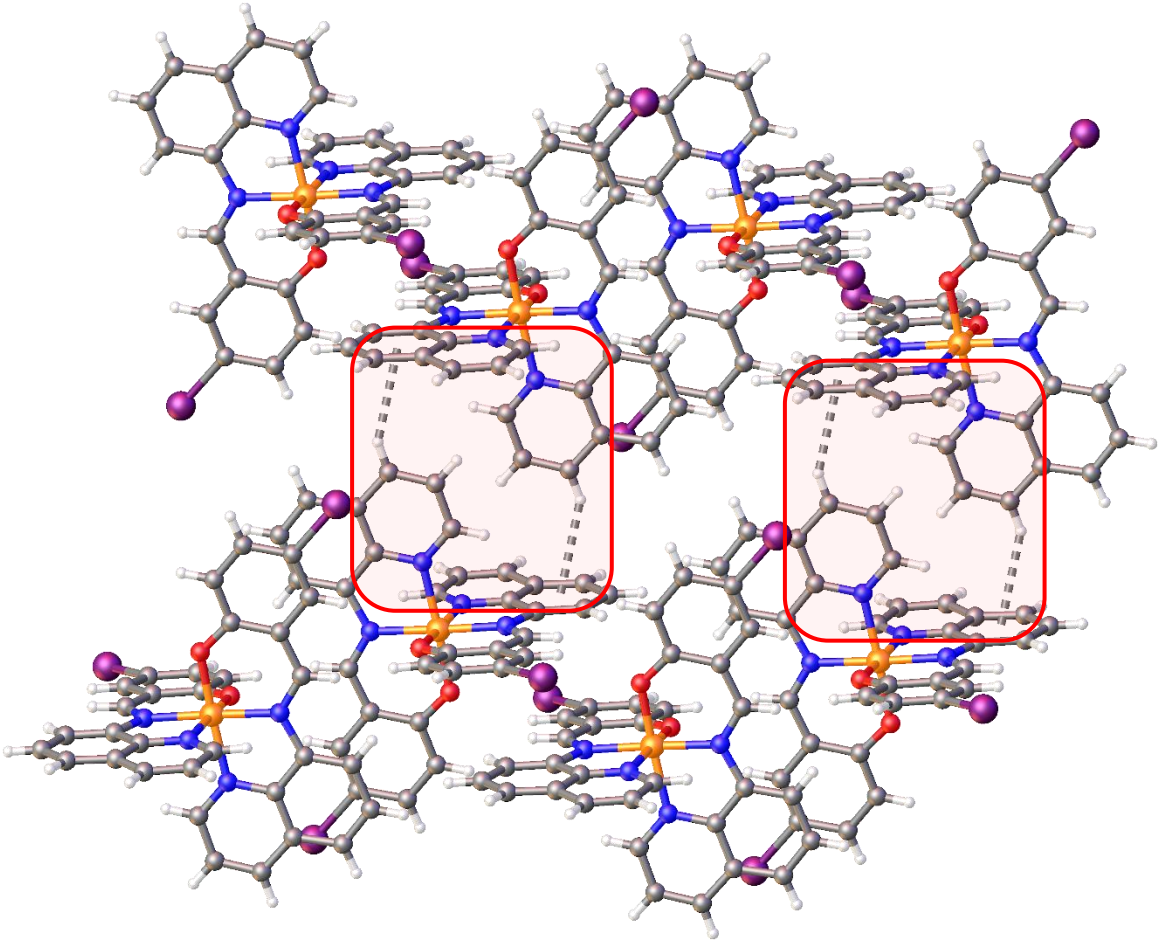

Figure S4 View of the pairs of C-H···π interactions that link the 1D chains into 2D sheets.

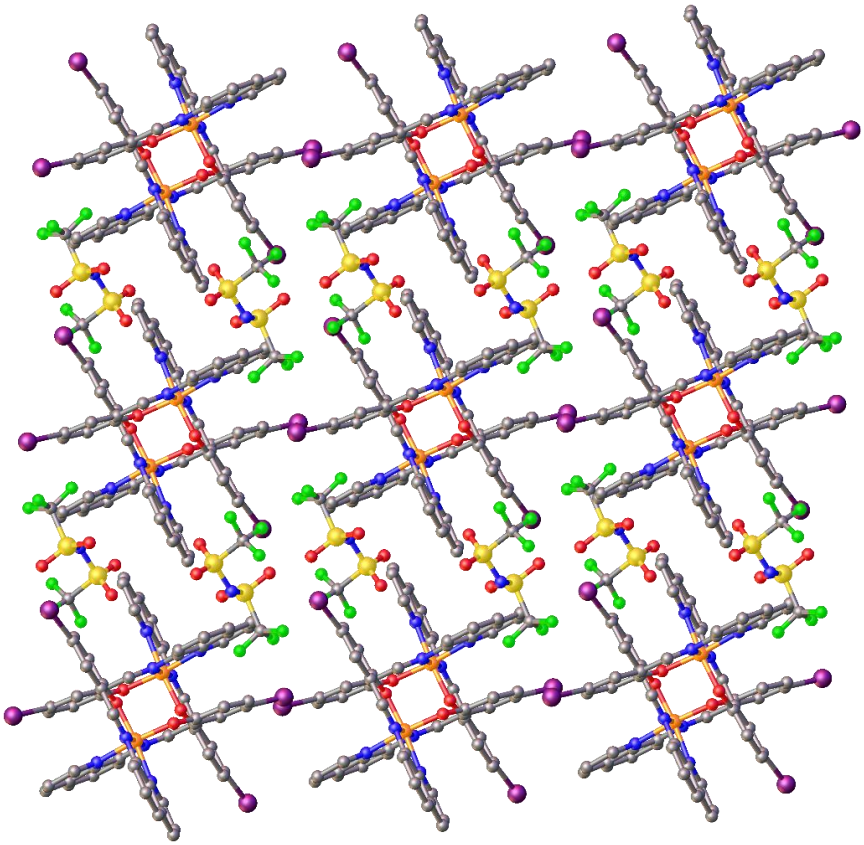

LS-245 K

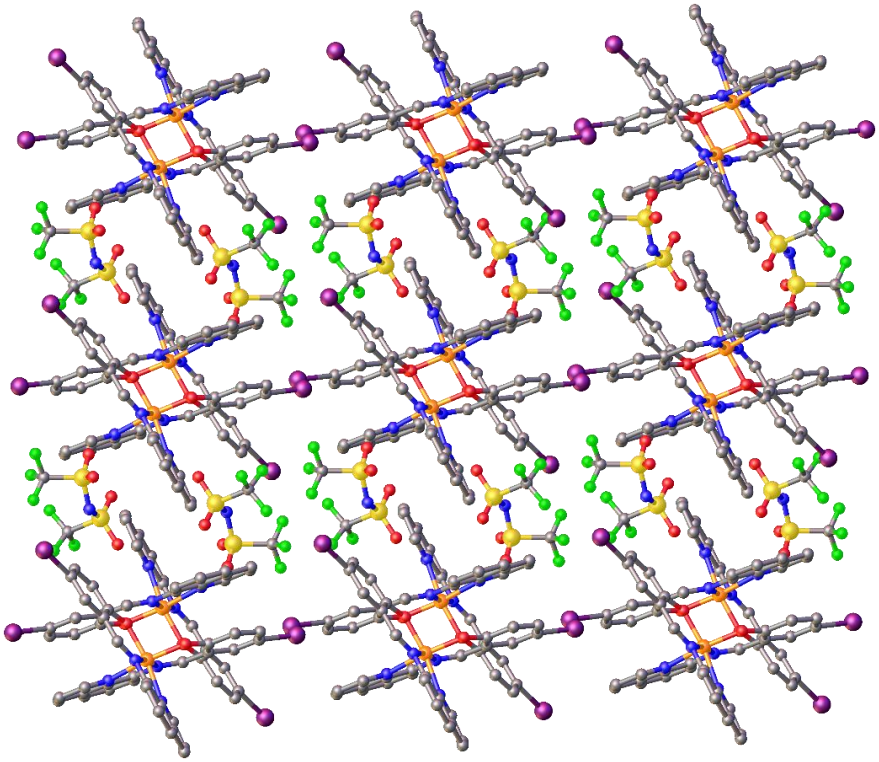

HS-255 K

Figure S5 View of the packing in $[Fe(qsal\text{-}I)_2]NTf_2$.

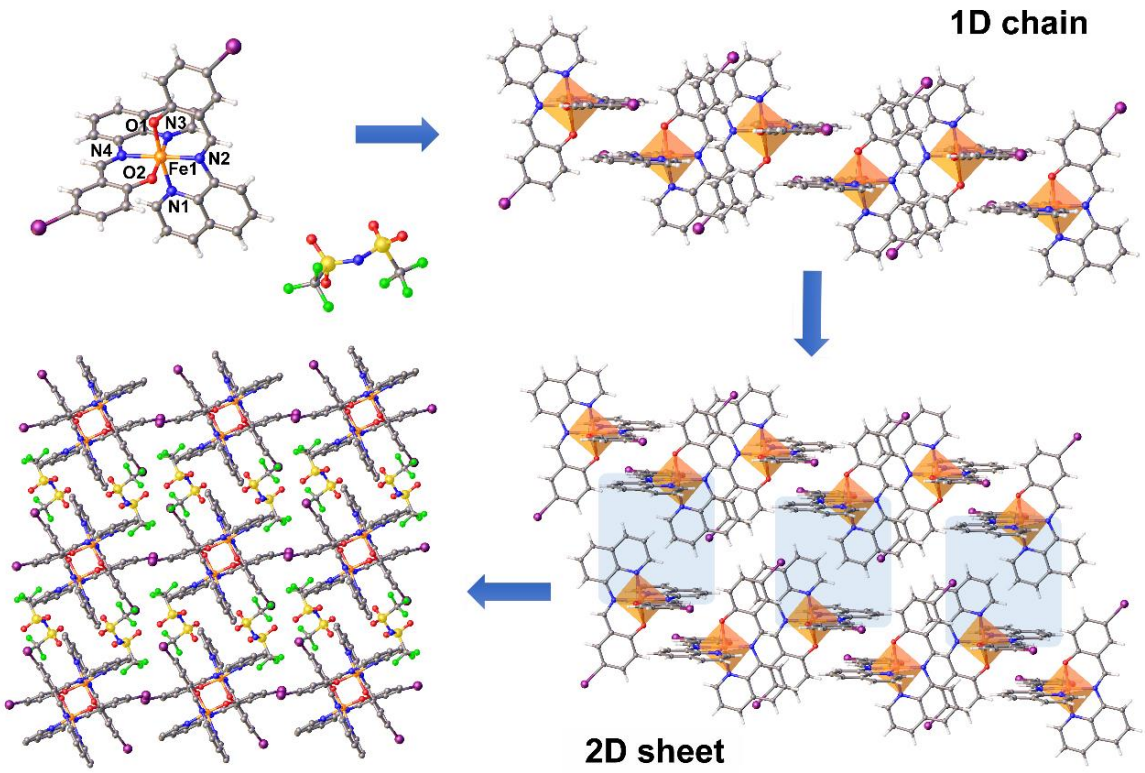

Figure S6 View of the packing in **1** at 245 K showing how the individual Fe(III) centres are connected to form the 3D supramolecular network. The network in the bottom left hand corner is viewed down the 1D π-π chains shown in the top right hand corner which at 245 K are coincident with the *a* axis. The blue squares highlight the pairs of C-H···π interactions that link the 1D chains.

Variable temperature IR and Raman spectroscopic studies

Variable temperature IR spectra were recorded on an Agilent Cary 600 Series FTIR spectrometer and microscope. For variable temperature Raman, the experiments were performed on a *Renishaw Invia* Raman microscope with excitation at wavelength of 633 nm at a regular (low) confocal setting with 500 microwatts delivered onto the sample mounted inside a *Linkam FTIR600* temperature controlled stage. The spectra were recorded in one extended range scan 200 cm^{-1} to 2001 cm^{-1} shift at rate of 30sec. The temperature of a small crystal sitting atop a 0.2mm thick glass coverslip was allowed to equilibrate for 20 sec before each scan was initiated.

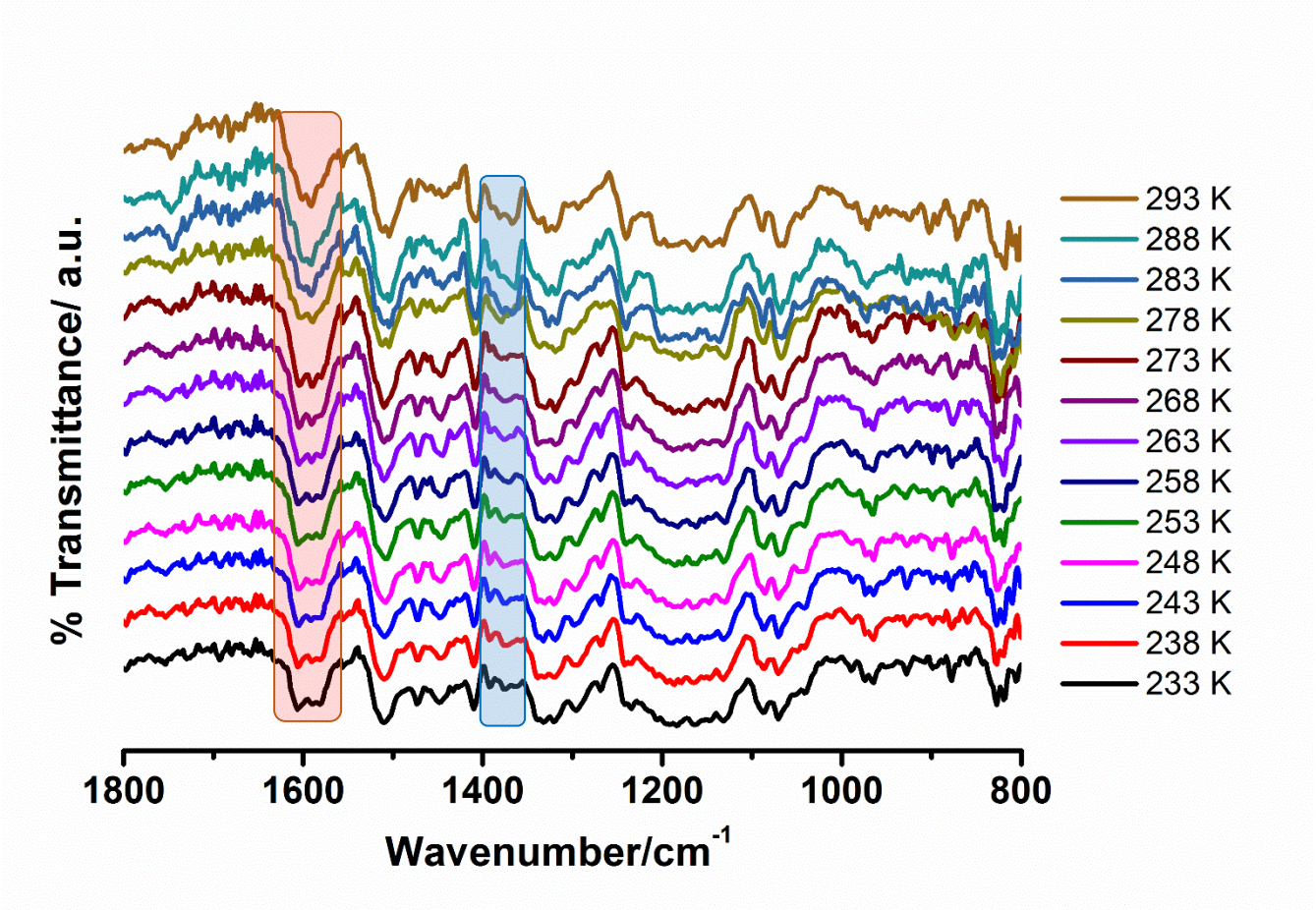

Figure S7 VT-IR spectra upon cooling from 293 to 233 K between 800-1800 cm^{-1}. The changes in the imine C=N stretches are highlighted in red while S=O stretches are highlighted in blue.

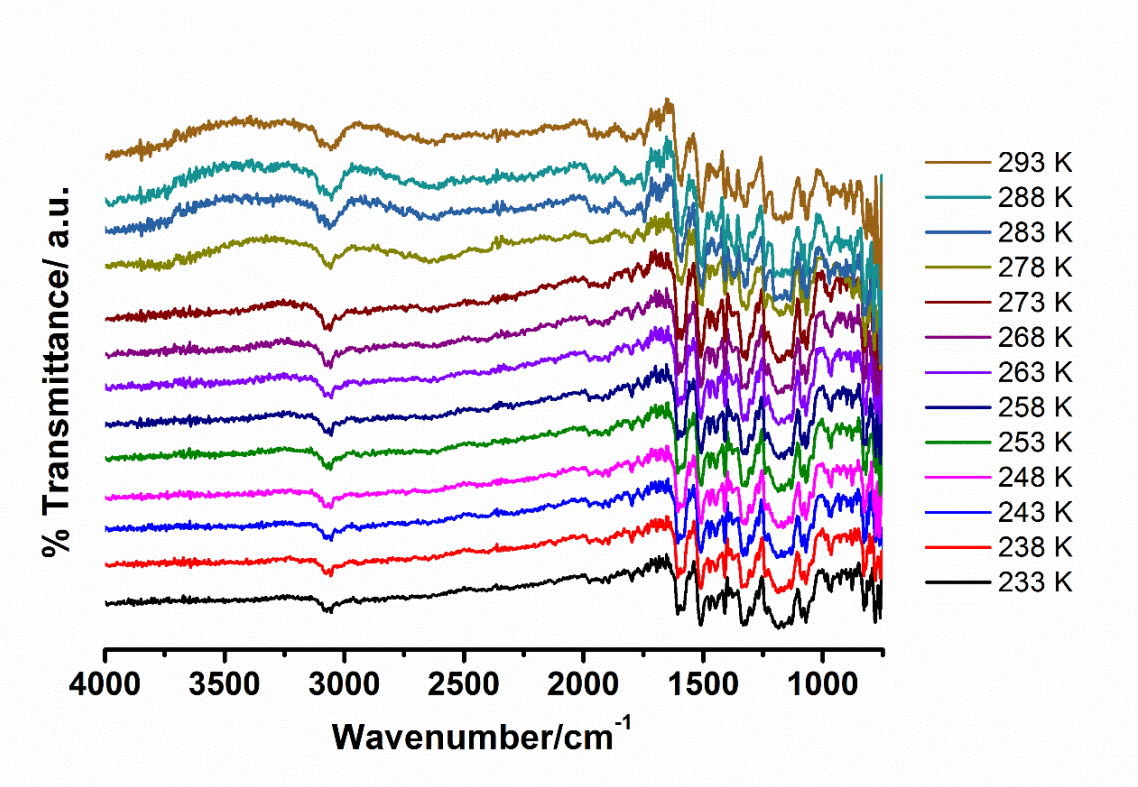

Figure S8 VT-IR spectra upon cooling from 293 to 233 K between 500-4000 cm^{-1}.

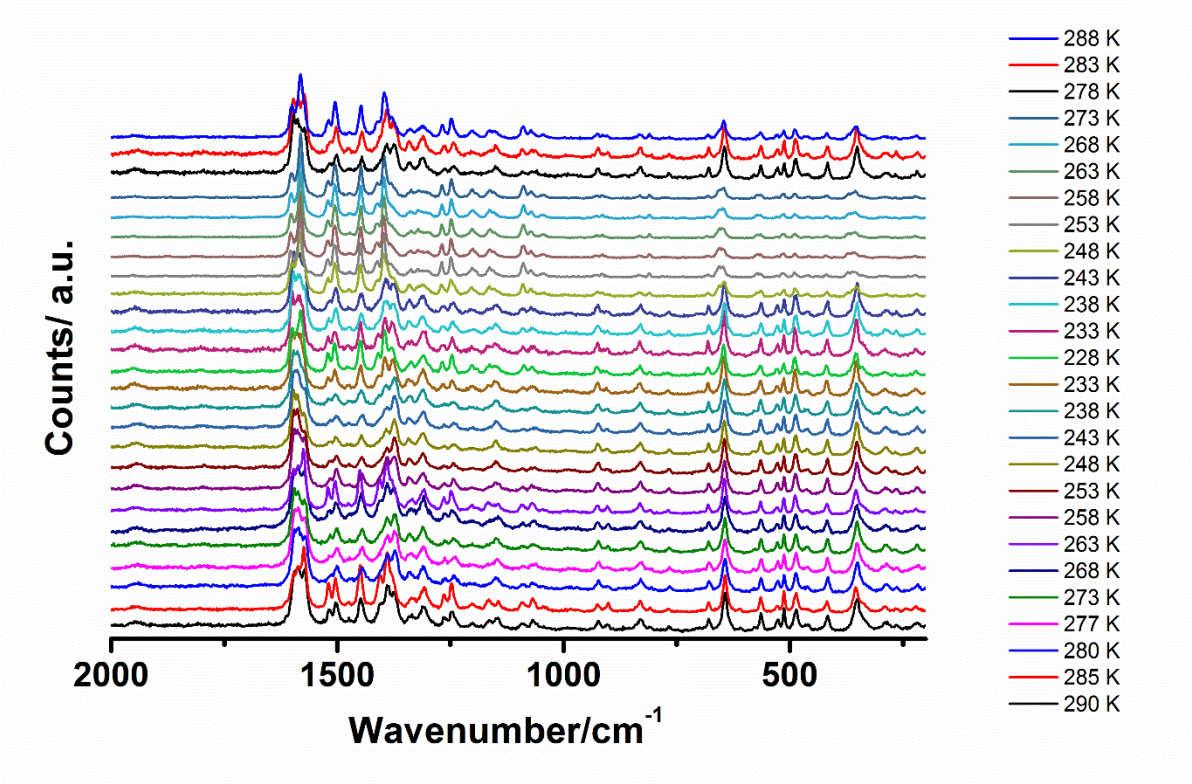

Figure S9 Variable temperature Raman spectra from 290 K → 228 K → 288 K in the cooling and heating modes.

References

1 J. Sirirak, W. Phonsri, D. J. Harding, P. Harding, P. Phommon, W. Chaoprasa, R. M. Hendry, T. M. Roseveare and H. Adams, *J. Mol. Struct.*, 2013, **1036**, 439–446.

2 S. Hayami, Z.-Z. Gu, H. Yoshiki, A. Fujishima and O. Sato, *J. Am. Chem. Soc.*, 2001, **123**, 11644–50.

3 S. Hayami, K. Hiki, T. Kawahara, Y. Maeda, D. Urakami, K. Inoue, M. Ohama, S. Kawata and O. Sato, *Chem. Eur. J.*, 2009, **15**, 3497–3508.

4 K. Takahashi, T. Sato, H. Mori, H. Tajima, Y. Einaga and O. Sato, *Hyperfine Interact.*, 2012, **206**, 1–5.

5 W. Phonsri, P. Harding, L. Liu, S. G. Telfer, K. S. Murray, B. Moubaraki, T. M. Ross, G. N. L. Jameson and D. J. Harding, *Chem. Sci.*, 2017, **8**, 3949–59.

6 M. Nakaya, K. Shimayama, K. Takami, K. Hirata, A. S. Alao, M. Nakamura, L. F. Lindoy and S. Hayami, *Chem. Lett.*, 2014, **43**, 1058–1060.

7 S. Floquet, M.-L. Boillot, E. Rivière, F. Varret, K. Boukheddaden, D. Morineau and P. Négrier, *New J. Chem.*, 2003, **27**, 341–48.

8 S. Kang, Y. Shiota, A. Kariyazaki, S. Kanegawa, K. Yoshizawa and O. Sato, *Chem. - A Eur. J.*, 2016, **22**, 532–538.

9 E. W. T. Yemeli, G. R. Blake, A. P. Douvalis, T. Bakas, G. O. R. Alberda van Ekenstein and P. J. van Koningsbruggen, *Chem. Eur. J.*, 2010, doi: 10.1002/chem.201002100.

10 S. Floquet, E. Rivière, K. Boukheddaden, D. Morineau and M. L. Boillot, *Polyhedron*, 2014, **80**, 60–68.

11 B. Weber, W. Bauer and J. Obel, *Angew. Chem. Int. Ed.*, 2008, **47**, 10098–10101.

12 C. Lochenie, W. Bauer, A. P. Railliet, S. Schlamp, Y. Garcia and B. Weber, *Inorg. Chem.*, 2014, **53**, 11563–11572.

13 E. Tailleur, M. Marchivie, N. Daro, G. Chastanet and P. Guionneau, *Chem. Commun.*, 2017, **53**, 4763–4766.

14 CrysAlis^{Pro}, Rigaku Oxford Diffraction, 2017, version: 1.171.39.13a, Rigaku Corporation, Oxford, UK.

15 G. M. Sheldrick, *Acta Crystallogr. Sect. A Found. Crystallogr.*, 2015, **71**, 3–8.

16 G. M. Sheldrick, *Acta Crystallogr. Sect. C Struct. Chem.*, 2015, **71**, 3–8.

17 O. V. Dolomanov, L. J. Bourhis, R. J. Gildea, J. A. K. Howard and H. Puschmann, *J. Appl. Cryst.*, 2009, **42**, 339–42.